NUMERICAL AND EXPERIMENTAL SIMULATION OF DAMAGE BEHAVIOUR OF FIBRE METAL LAMINATES

Peter Linde*, Jürgen Pleitner*, Henk de Boer, Jos Sinke*****
***Airbus, Hamburg, Germany, **Advanced Lightweight Engineering, Delft, The Netherlands, ***Faculty of Aerospace Engineering, Delft Technical University, Delft, The Netherlands**

Keywords: *Fibre Metal Laminates, Fracture Energy, Numerical Model, Damage Behaviour*

Abstract

Fibre Metal Laminates (FML) are becoming important as aircraft fuselage skin material as an alternative to monolithic aluminium. FML consists of a built-up material, comprising thin layers of aluminium alternated by layers of glass fibres.

The paper deals with a microscopic model based on the finite element method for simulating the damage behaviour of FML. *Each of the layers is modelled by solid elements, and the interlaminar behaviour is modelled by an interface model. Each physical damage mechanism is modelled separately. The damage mechanisms comprise: interlaminar delamination, fibre failure and matrix cracking.*

This paper focuses on delamination behaviour. In order to validate the numerical model an experimental test is performed for interlaminar delamination. This test is described in the paper. Numerical analysis results obtained with the developed model are compared with the test results and discussed. The model is used in an applied example and a summary and conclusions are given.

1 Introduction

A family of material that has obtained increased use in aircraft structures during recent years constitutes the fibre metal laminates. This hybrid material consists of alternating layers of aluminium and glass fibre reinforced epoxy and displays improved characteristics in terms of fatigue behaviour, fire resistance and damage behaviour [1].

This paper treats a numerical model to simulate the damage behaviour of fibre metal laminates. Different failure mechanisms are modelled separately, such as aluminium plasticity, interlaminar delamination, fibre failure and matrix cracking. Focus in this paper is placed on interlaminar delamination behaviour [2].

To validate the numerical model an experimental test is performed and described. The test determines the interlaminar behaviour by peeling apart the material at the interface between two layers. Focus is placed in tensile behaviour by means of a so called “mode I” test. Amongst the test results is the fracture energy. In the numerical model the interlaminar delamination behaviour is described by a separate model which is fracture energy based. Comparison between numerical and experimental results are performed and discussed.

The paper is organized as follows. Upon this introduction the experimental test for interlaminar behaviour is treated. The test setup is described and the performance of the tests are explained. Thereafter the numerical model is presented and its different damage mechanisms are discussed. Finally, comparison of experimental and numerical results are presented, and a summary, and conclusions are given.

2 Experimental test for interlaminar delamination

To understand the damage behaviour of the laminated material and to validate the numerical model, experimental tests were

performed [3] according to AITM standards [4], based on a similar ASTM-standard.

Delamination may occur between two layers in the material and may occur in a tensile mode (mode I), in a shear mode (mode II), or a mode consisting of both tensile and shear (mixed mode). Figure 1 shows the test set-up

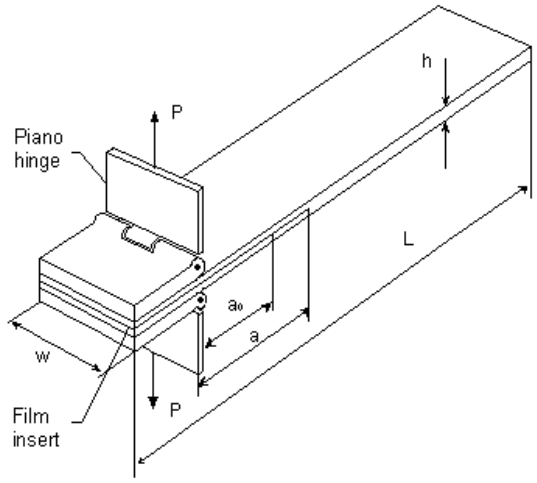

Fig. 1. Test Principle for the Interlaminar Dela-mination Peel Test in Mode I.

for a mode I test. The test specimen consists of a rectangular material strip which is peeled apart at the interface between two layers. An artificial crack is implemented in the specimen in the form of a thin teflon sheet placed between two material layers. By a force pulling on a hinge attached to the top surface of the specimen right above the end of the teflon insert the specimen is peeled apart over a prescribed length

As results are obtained the global force-cross head displacement curve. The mode I fracture energy is obtained by the shaded area in the picture divided by the cracked area in the specimen.

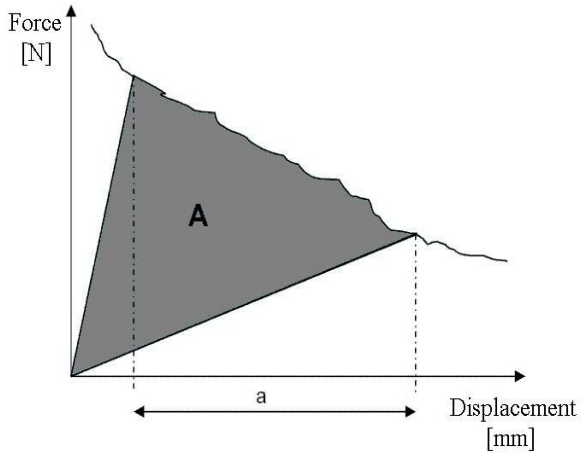

Fig. 2. Force-Cross Head Displacement, Mode I Fracture Energy: Shaded Area Divided by the Cracked Area in the Specimen.

Thus the fracture toughness energy is calculated by

$$G_{Ic} = \frac{A}{a \cdot w}$$

where:

G_{Ic} the fracture toughness energy
A the energy to achieve the total propagated crack length – see figure 2
a the propagated crack length – see figure 3
w width of the specimen.

Fig. 3. Test specimen: hinges attached (left), white fluid painted on edge for crack growth monitoring

For interlaminar delamination behaviour in a shear mode (mode II) corresponding tests were performed. The test principle is illustrated in figure 4 and is of the ENF-type (end–notched flexure)

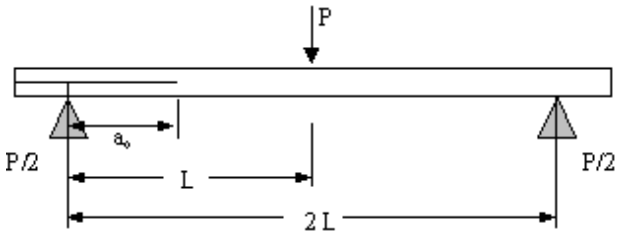

Fig. 4. Test principle for mode II tests

The G_{IIc}-value can be calculated with:

$$G_{II,c} = \frac{9Pa^2d}{2w\left(0.25L^3 + 3a^3\right)}$$

where a denotes the initial crack length, P the limit load, d the cross-head displacement, w the width of the specimen and L the span length.

3. Numerical Model

The numerical model uses solid elements for modelling the separate layers. The delamination behaviour can be treated either with a special interface element (see figure 5), or by means of a user subroutine UINTER in the program ABAQUS®. The latter option is chosen here since it allows for non congruent meshes and is part of a contact formulation.

The fibre failure and matrix cracking in the glass fibre reinforced prepreg layer are treated by the user material subroutine UMAT in ABAQUS. These damage models are discussed separately in the following. The damage behaviour is modelled separately and divided into plasticity in the aluminium, delamination between layers, and fibre failure and matrix cracking in the prepreg.

The interlaminar damage behaviour is described in the following. Failure in this model is related to the equivalent relative displacement, κ, based on [5], and is defined by the following formulation

$$\kappa = \sqrt{u_1^2 + \left(\frac{u_{ft}}{u_{fs}}\right)^2 u_2^2 + \left(\frac{u_{ft}}{u_{fs}}\right)^2 u_3^2},$$

where u_{ft} is the gap opening displacement leading to failure and u_{fs} denotes the maximum shear displacement. Failure will occur when $\kappa > u_{ft}$. Notice that the failure function is based on relative displacements. The stiffness of the interface is taken equal to the stiffness

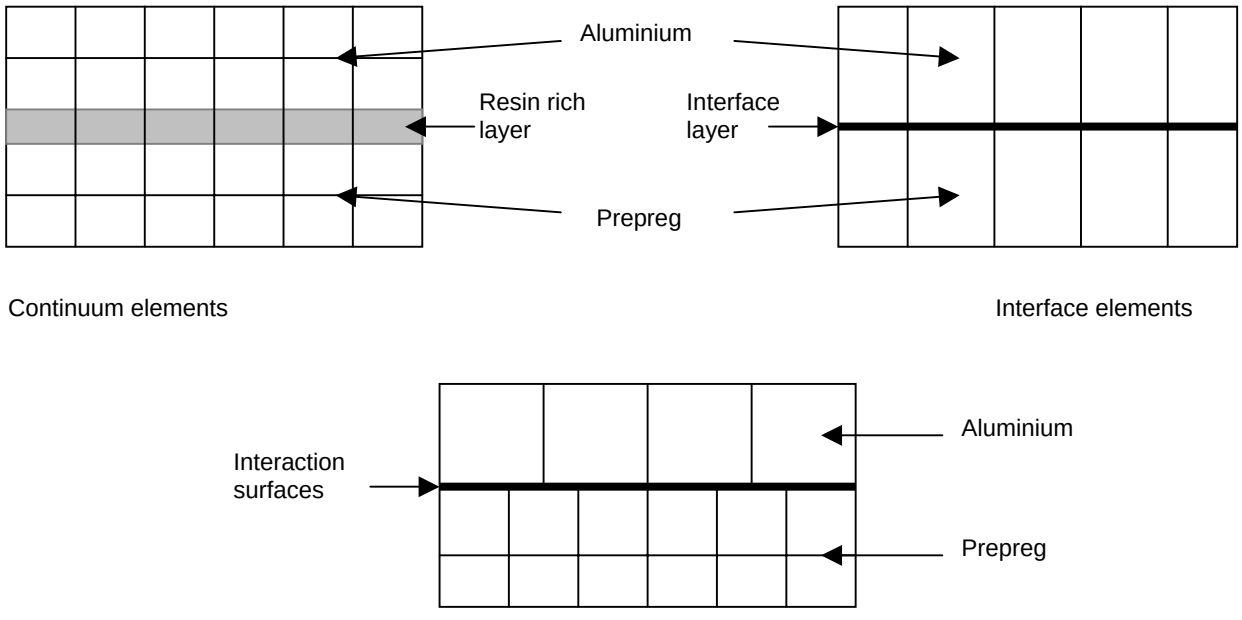

Fig. 5. Modelling of fibre metal laminate

of the matrix material. The strength of the interface is taken from experimental results. This leads to

$$u_{ft} = \frac{\sigma_{t,\max}}{E \cdot t}, \text{ and } u_{fs} = \frac{\tau_{\max}}{G \cdot t}.$$

Here t denotes the thickness of the resin rich layer, E modulus, G modulus and maximum stresses relate to the matrix material.

In case of damage the elastic properties of the interface will reduce. The damage parameters are defined as

$$d_1 = 1 - \frac{u_{ft}}{\kappa} e^{\left(-C_{11} u_{ft} (\kappa - u_{ft})/G_{c,I}\right)},$$

$$d_2 = 1 - \frac{u_{ft}}{\kappa} e^{\left(-C_{22} u_{fs}^2 (\kappa - u_{ft})/(G_{c,II} \cdot u_{ft})\right)},$$

$$d_3 = 1 - \frac{u_{ft}}{\kappa} e^{\left(-C_{33} u_{fs}^2 (\kappa - u_{ft})/(G_{c,II} \cdot u_{ft})\right)},$$

where $G_{c,I}$ and $G_{c,II}$ denote the fracture energy per unit area for mode I and mode II in [N/mm], respectively. The modulus stiffnesses read

$$C_{11} = \frac{E}{\tau}, \quad C_{22} = \frac{G}{\tau}, \quad C_{33} = \frac{G}{\tau}.$$

Notice that damage parameters are equal to zero if $\kappa > u_{ft}$. The relation between relative displacements and tractions is given by

$$\begin{bmatrix} t_1 \\ t_2 \\ t_3 \end{bmatrix} = \begin{bmatrix} (1-d_1)C_{11} & 0 & 0 \\ 0 & (1-d_2)C_{22} & 0 \\ 0 & 0 & (1-d_3)C_{33} \end{bmatrix} \begin{bmatrix} u_1 \\ u_2 \\ u_3 \end{bmatrix}$$

Notice that the failure function κ and the damage parameters d_i cannot be chosen independently, since

$$\int_0^{uft} t_1 du_1 = G_{c,I}$$

must hold true (compare figure 2). A similar relation applies for $G_{c,II}$.

For matrix failure in the prepreg the following failure criterion is used.

$$f_m = \sqrt{\frac{\varepsilon_{22}^t}{\varepsilon_{22}^c}(\varepsilon_{22})^2 + \left(\varepsilon_{22}^t - \frac{(\varepsilon_{22}^t)^2}{\varepsilon_{22}^c}\right)\varepsilon_{22} + \left(\frac{\varepsilon_{22}^t}{\varepsilon_{12}^s}\right)^2 (\varepsilon_{12})^2}$$

where ε_{22}^t and ε_{22}^c are the failure strains perpendicular to the fibre direction in tension and compression, respectively. The failure strain for shear is ε_{12}^s. Failure occurs when f_m exceeds its threshold value ε_{22}^t.

In case of damage, a damage parameter is calculated as follows

$$d_m = 1 - \frac{\varepsilon_{22}^t}{f_m} e^{\left(-C_{22}\varepsilon_{22}^t (f_m - \varepsilon_{22}^t)/G_m\right)}.$$

The glass/epoxy layer shows transverse isotropy. Therefore, the modulus stiffnesses read

$$C_{11} = \frac{E_L(1-\nu_{TT}^2)}{a}; \qquad C_{22} = \frac{E_T(1-\nu_{LT}\nu_{TL})}{a};$$

$$C_{33} = \frac{E_T(1-\nu_{LT}\nu_{TL})}{a}$$

$$C_{12} = \frac{E_T(\nu_{LT}-\nu_{LT}\nu_{TT})}{a};$$

$$C_{13} = \frac{E_T(\nu_{LT}-\nu_{LT}\nu_{TT})}{a}; \quad C_{23} = \frac{E_T(\nu_{TT}-\nu_{LT}\nu_{TL})}{a}$$

$$C_{44} = G_{LT}; \qquad C_{55} = G_{LT}; \qquad C_{66} = G_{TT},$$

with

$$a = 1 - 2\nu_{LT}\nu_{TL} - \nu_{TT}^2 - 2\nu_{LT}\nu_{TL}\nu_{TT}.$$

The failure criterion for fibre failure [6] is given by

$$f_f = \sqrt{\frac{\varepsilon_{11}^t}{\varepsilon_{11}^c}(\varepsilon_{11})^2 + \left(\varepsilon_{11}^t - \frac{(\varepsilon_{11}^t)^2}{\varepsilon_{11}^c}\right)\varepsilon_{11}}.$$

Here ε_{11}^t and ε_{11}^c are the failure strains in fibre direction in tension and compression, respectively. Failure occurs when f_f exceeds its threshold value ε_{11}^t.

A second damage parameter for fibre damage is introduced

$$d_f = 1 - \frac{\varepsilon_{11}^t}{f_f} e^{\left(-C_{11}\varepsilon_{11}^t (f_f - \varepsilon_{11}^t)/G_f\right)}.$$

The modulus matrix of the glass/epoxy layer will be reduced according to

$$C = \begin{bmatrix} (1-d_f)C_{11} & (1-d_f)(1-d_m)C_{12} & (1-d_f)C_{13} & 0 & 0 & 0 \\ & (1-d_m)C_{22} & (1-d_f)(1-d_m)C_{23} & 0 & 0 & 0 \\ & & C_{33} & 0 & 0 & 0 \\ & & & (1-d_f)(1-d_m)C_{44} & 0 & 0 \\ & & & & C_{55} & 0 \\ sym & & & & & C_{66} \end{bmatrix}$$

The stresses are computed by

$$\bar{\sigma} = C \cdot \bar{\varepsilon}.$$

4 Results

The numerical model utilizes the fracture energies delivered by the test results. These energies are to be viewed as a material characteristic. The mode I fracture toughness energy G_{Ic} for the tested FML of type Glare® 3 was taken from the tests with an average value of 4 N/mm, and implemented in the model. The model delivered a numerical result seen in figure 6. This is in good agreement with the test results seen in the same figure. The reason is explained by the fact the mode I test delivers a stable crack propagation and it is possible to measure it until the end. Therefore the global fracture toughness energy can be calculated by the equation given in section two.

In the numerical model an interface peel strength of 50 MPa was assumed. It may be seen in figure 7 that most of the elements display a consumed fracture energy close to 4 N/mm over most of the cracked area, even towards the right end.

The mode II test used here is of the end-notched flexure (ENF) type, which does not give a fully stable crack propagation. The fracture toughness energy G_{IIc} resulting from

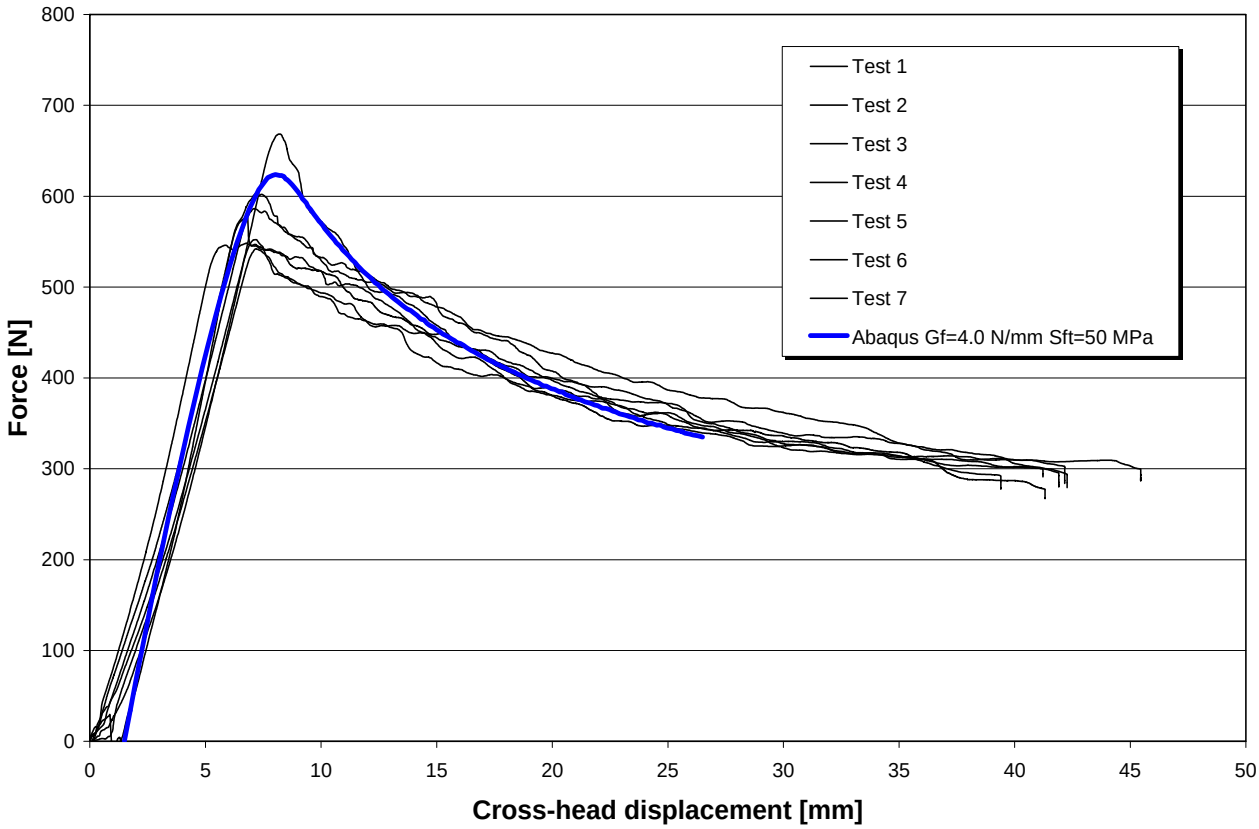

Fig. 6. Computed results for mode I by ABAQUS and test results

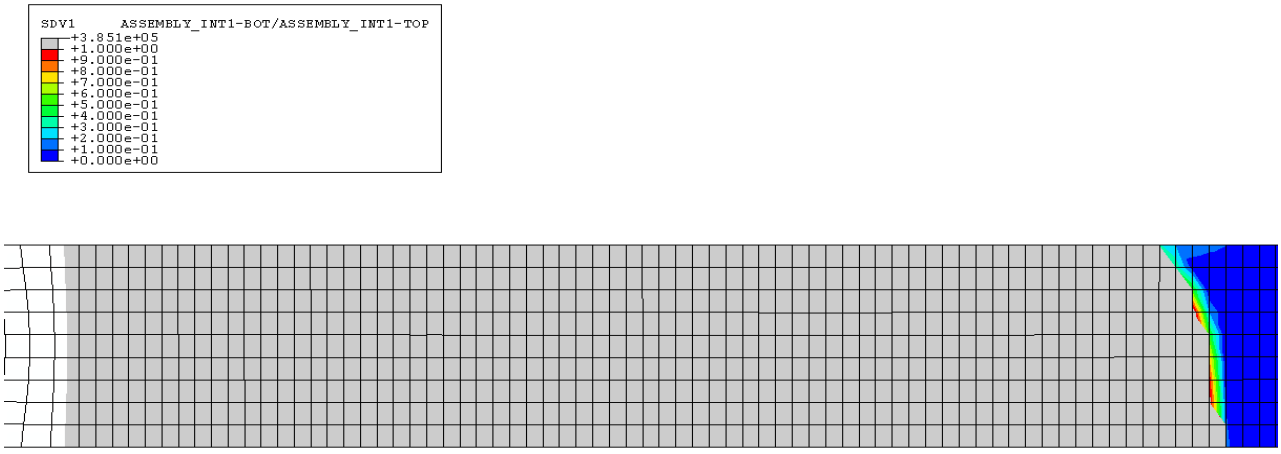

Fig. 7. Fracture energy consumed in numerical model; mode I test simulation

the test described in section 2 should be understood as a global value. Values of the test averaged around 2 N/mm for Glare3. It should be noted that the crack stops at the centre of the specimen and there is a non uniform distribution of cross head displacement and locally consumed fracture energy.

Figure 8 shows numerical results for mode II compared with tests results. Inserting G_{IIc}, according to the formula in section two with values from the test, directly into the model delivers a conservative estimation of the load carrying capacity. The reason lies in the fact that no even distribution of consumed fracture energy takes place in the ENF test.

A fracture energy comparable to mode I, amounting to 4 N/mm, is used as well in the simulations as seen in figure 8. This delivers

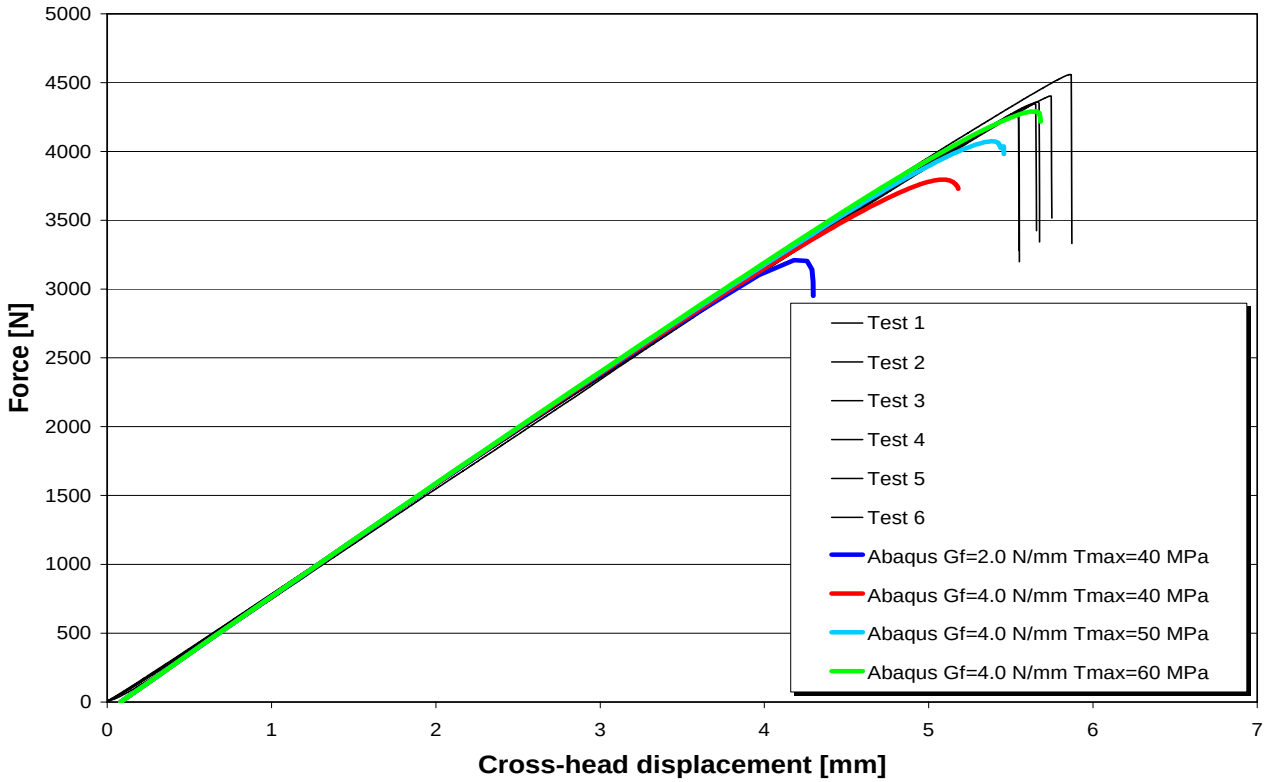

Fig. 8. Computed results for mode II by ABAQUS and test results

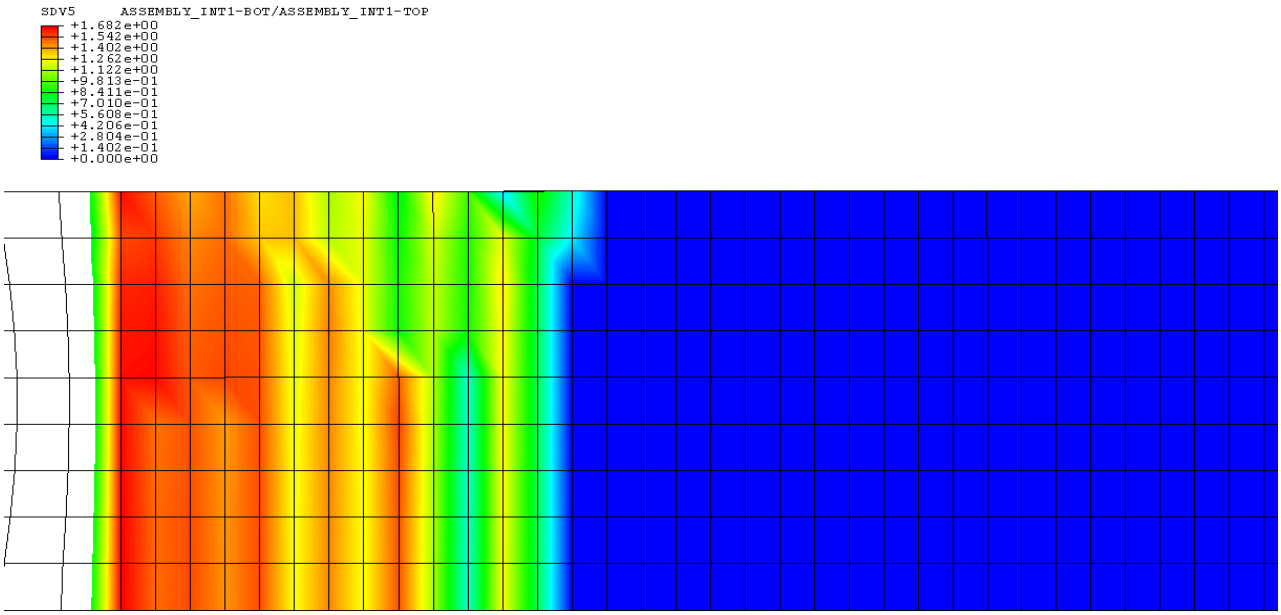

Fig. 9. Fracture energy consumed in numerical model; mode II test simulation

more realistic results, and corresponds to a global fracture toughness energy of around 2 N/mm due to the uneven distribution. The shear strength also has an effect on the simulation result as seen from the numerical curves in Figure 8.

The distribution of consumed fracture energy is shown in figure 9 for an entered value of 2 N/mm (high consumption only at the leftmost end), resulting in a too low average fracture energy, whereas entering a value of 4 N/mm resulted in an average fracture energy corresponding to the test value. In real aircraft conditions typically a mode mixed between mode I and II may occur and mixed mode tests and simulations were treated as well, not described here.

The numerical model developed thus has been used in practical research. One such example is displayed in figure 10 in the form of a model of a so called Inter Rivet Buckling (IRB) problem [7]. In this problem an axial force is applied to an FML specimen riveted to stiffener plates by rivets [8].

With proper modeling of the boundary condition, and calibrated with fracture energy values from the tests as discussed above (4 N/mm for both mode I and II) the model was

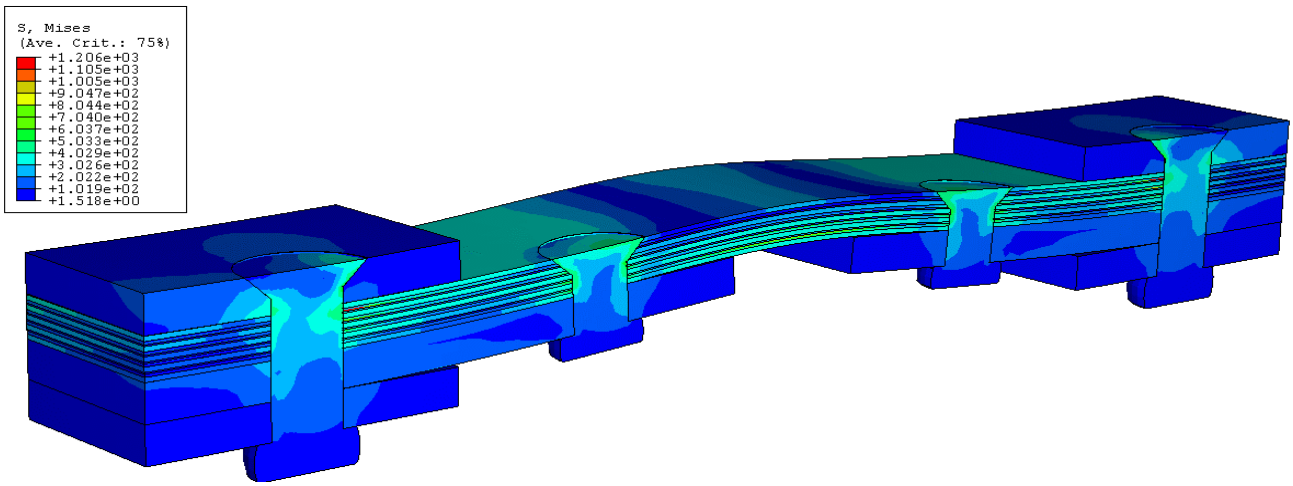

Fig. 10. Model of the Inter Rivet Buckling test, simulated by the numerical model developed

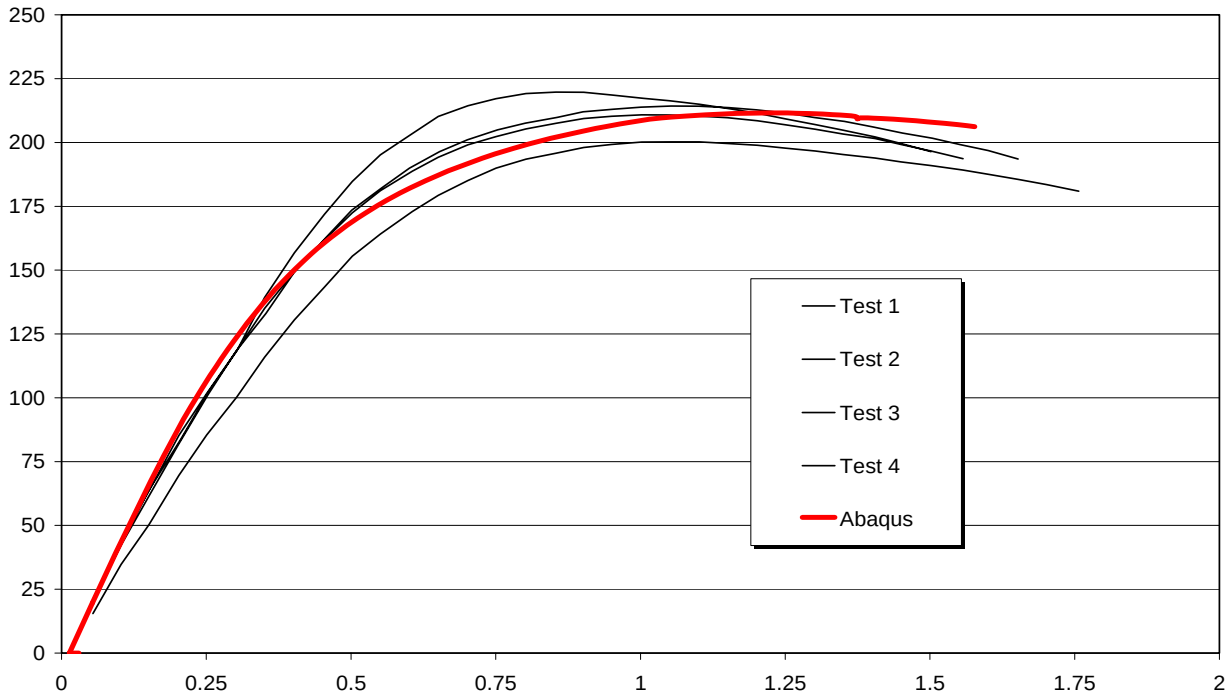

Fig. 11. Inter rivet buckling; test and numerical results

able to realistically predict the non linear behaviour of the inter rivet buckling test including delamination occurring at the end after reaching maximum load, [8] (figure 11).

5. Summary and Conclusions

In this study the experimental tests for determination of the fracture toughness energies in modes I and II were presented. A detailed numerical model for fibre metal laminates was presented, based on solid elements for each layer and with separate fracture energy based failure mechanisms for delamination, fibre failure and matrix cracking. The calibration of the model with fracture toughness energy values from the tests was discussed and the realistic prediction of the applied inter rivet buckling problem demonstrated. The following conclusion can be drawn:

- a numerical model for simulation of the damage behaviour of fibre metal laminates should contain a realistic model for delamination
- the fracture energy values from the mode I and mode II tests, as implemented in the model, resulted in a realistic prediction of the force-deformation behaviour of these tests
- the model was applied in an realistic prediction of the load carrying capacity in the inter rivet buckling problem
- using the test results, it could be demonstrated that no delamination would occur under real aircraft conditions.

Acknowledgements

Dr. Clarice Carmone of Bishop Aeronautical Engineers, Hamburg, is acknowledged for finalizing the manuscript, and for careful proof reading.

References

[1] Vlot A., Gunnink J. W. *Fibre Metal Laminates - An introduction*, Kluwer Academic Publishers, 2001.

[2] Sinke J., Van de Brande J. *Numerical modelling of fibre metal laminate: microscopic damage models.* Internal Report, Airbus Industrie, 2003.

[3] de Boer H. *Numerical modelling of fibre metal laminate: microscopic damage models.* Internal Report, Airbus Industrie, 2003.

[4] AITM 1.0005, AITM 1.0006. Airbus Industries Test Method, *Fibre Reinforced Plastics, Determination of Interlaminar Fracture Toughness Energy, Mode I, Mode II*, Airbus Industrie, 1994.

[5] Schipperen J. H. A. *Computational modelling of failure in fibre reinforced plastic.* Delft University of Technology, 2001.

[6] Zemičik R., Laš V. *Numerical model for progressive failure of analysis of fibre-reinforced composite laminate,.* Internet, Thesis, Université Pierre et Marie Curie, Cachan, France 1992.

[7] Linde P., Pleitner J, de Boer H, Carmone C. *Modelling and Simulation of FML*, ABAQUS Users Conference, Boston, 25-27 May, 2004.

[8] Ypma M. S. *Exploratory compression strength tests on skin details.* Report B2V-00-59, Delft University of Technology, 2001.